Palaeogeography, Palaeoclimatology, Palaeoecology 618 (2023) 111512

Contents lists available at ScienceDirect

Palaeogeography, Palaeoclimatology, Palaeoecology

journal homepage: www.elsevier.com/locate/palaeo

An example of the Middle to Late Devonian marine nitrogen cycle from mudstones of the Horn River Group, Northwest Territories, Canada

Maya T. LaGrange [a,*], Kan Li [a,b], Long Li [a], Pavel Kabanov [c,d], Kurt O. Konhauser [a], Brette S. Harris [a], Sara K. Biddle [a], Viktor Terlaky [e], Murray K. Gingras [a]

[a] University of Alberta, Department of Earth and Atmospheric Sciences, 1-26 Earth Sciences Building, Edmonton, AB T6G 2E3, Canada
[b] Woods Hole Oceanographic Institution, MC&G Dept., Woods Hole, MA 02543, USA
[c] Geological Survey of Canada, 3303 33 St NW, Calgary, AB T2L 2A7, Canada
[d] University of Calgary, Department of Geoscience, 2500 University Drive NW Calgary, AB T2N 1N4, Canada
[e] Northwest Territories Geological Survey, 4601 52nd Ave, Yellowknife, NT X1A 1K3, Canada

ARTICLE INFO

Editor: Dr A Dickson

Keywords:
Organic-rich mudstone
Black shale
Devonian
Marine nitrogen cycle
Redox

ABSTRACT

The Middle to Late Devonian was characterized by the widespread deposition of organic-rich mudstone units and successive biotic crises and anoxic events in the marine realm, the cause of which remains debated and requires constraints from associated marine conditions. This study provides an example of the marine nitrogen cycle throughout the late Eifelian to middle Frasnian anoxic pulses. We present new and previously published organic whole-rock N ($\delta^{15}N_{bulk}$) and carbon ($\delta^{13}C_{org}$) isotopic datasets from organic-rich mudstone units of the Horn River Group (Canol and Hare Indian Formations) and overlying Imperial Formation in the Central Mackenzie Valley, Northwest Territories, Canada. In the ConocoPhillips Mirror Lake N-20 core, $\delta^{13}C_{org}$ ranges from −31.0 ‰ to −24.3 ‰ with $\delta^{15}N_{bulk}$ from −3.8 ‰ to +1.9 ‰, whereas the Husky Little Bear N-09 core is characterized by $\delta^{13}C_{org}$ from −31.0 ‰ to −27.2 ‰ and $\delta^{15}N_{bulk}$ from −2.0 ‰ to +5.9 ‰. The N isotopic signatures near 0 ‰ and a lack of $\delta^{15}N_{bulk}$ – $\delta^{13}C_{org}$ relationship are characteristic of N_2 fixation by primary producers. Regular oscillations in $\delta^{15}N_{bulk}$ are interpreted as the product of episodic, mild oxygenation events. Together, our $\delta^{13}C_{org}$ and $\delta^{15}N_{bulk}$ results suggest that locally, N_2 fixation was the dominant source of N for primary producers in the late Eifelian to middle Frasnian, despite fluctuations in $\delta^{13}C_{org}$ and global marine paleoredox. These findings contribute to our understanding of the nitrogen speciation and bioavailability associated with anoxic events, biotic crises, and widespread organic carbon burial in the Eifelian to Frasnian oceans.

1. Introduction

In this contribution, we present a record of nitrogen and carbon stable isotopes from a sedimentary unit in Northern Canada that spans the Middle to Late Devonian (latest Eifelian to Frasnian). The time interval was characterized by the widespread deposition of organic matter (OM)-rich mudstone (e.g., Klemme and Ulmishek, 1991; Ormiston and Oglesby, 1995) in conjunction with a series of global biotic events and crises characterized by faunal overturn (e.g., McGhee et al., 2013; Walliser, 1996). From the latest Eifelian to Late Frasnian, eleven global biotic events have been recognized, many of which have corresponding positive $\delta^{13}C$ isotope excursions, including the Kačák, Taghanic, Frasnes, Middlesex (*punctata*), and Kellwasser events (e.g., Becker et al., 2020). Global biotic events in the Middle to Late Devonian greatly impacted the tropical shallow marine realm, with extinctions and overturn associated with many species of reef builders (e.g., corals and stromatoporoids), trilobites, brachiopods, ostracods, and ammonoids (e.g., Copper, 2002; House, 1985; Walliser, 1996). Moreover, OM-rich mudstone units, with ages corresponding to Devonian biotic events, have been recognized in locations across North America, Europe, Russia, and Northern Africa (e.g., Fig. 1 of Kabanov and Jiang, 2020).

Successive episodes of globally expanded marine anoxia on continental shelves is generally accepted as the explanation for the occurrence of these Devonian OM-rich mudstone intervals and associated biotic events, although there is not yet consensus about the root cause (e.g., Carmichael et al., 2019; Lu et al., 2021; Walliser, 1996; Zambito et al., 2012). The corresponding positive $\delta^{13}C$ excursions are thought to be the product of eutrophication causing high biological productivity,

* Corresponding author.
E-mail address: maya1@ualberta.ca (M.T. LaGrange).

https://doi.org/10.1016/j.palaeo.2023.111512
Received 30 August 2022; Received in revised form 25 February 2023; Accepted 12 March 2023
Available online 14 March 2023

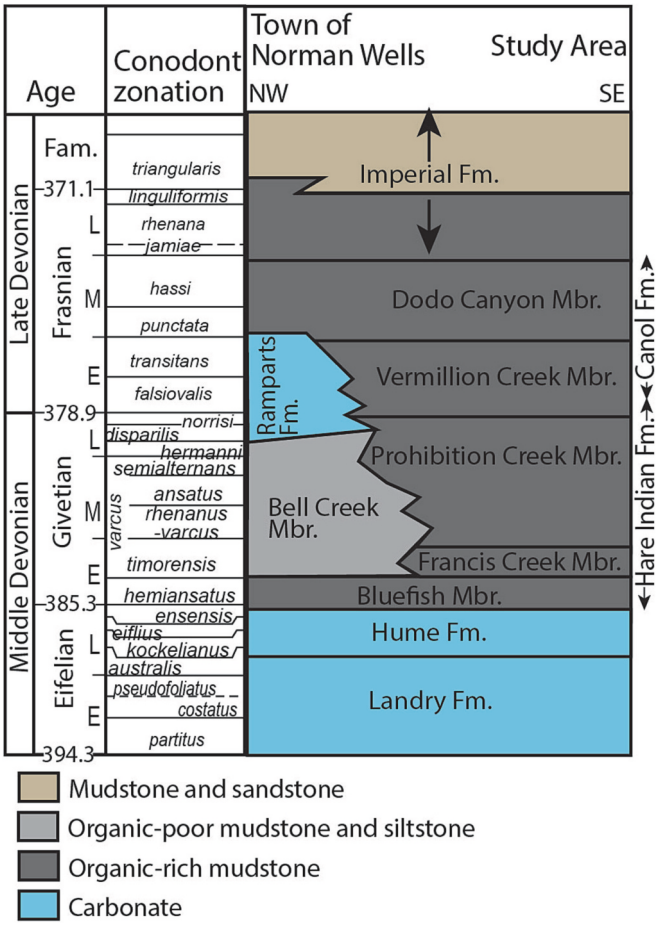

Fig. 1. Schematic stratigraphic column showing the Middle to Late Devonian units present in the central Mackenzie Valley, Northwest Territories, Canada. This chart is modified from Kabanov and Deblonde (2019) and adjusted to the most recent stage boundary calibrations from Becker et al. (2020). Members are shown for the Hare Indian and Canol Formations. This column shows the difference in stratigraphic units present from the area near the town of Norman Wells compared to our study area to the southeast. Abbreviations: Mbr–Member, Fm–Formation, Gp–Group. Binomial names of the conodont zones are included in Appendix A.

increased OM burial, and ultimately depletion of ^{12}C in the marine C reservoir (e.g., Murphy et al., 2000; Pisarzowska and Racki, 2012). For the Middle to Late Devonian, several triggers of high productivity have been proposed: most notably, eutrophication of epeiric seas from volcanism (Racki et al., 2018) and increased terrestrial weathering associated with either land plant evolution (Algeo and Scheckler, 1998) or intense mountain building (Averbuch et al., 2005). Murphy et al. (2000) also argued that eutrophication was maintained by fluctuating redox conditions, which led to the recycling of biolimiting nitrogen and phosphorus from anoxic seafloors.

A large body of research exists for the Frasnian –Famennian (Kellwasser) and end-Devonian (Hangenberg) mass extinction events, with significantly less focus on other global carbon-cycle perturbations, which are notably numerous in the Middle and Late Devonian, but not all of them associated with severe biotic crises (review in Becker et al., 2020). Knowledge of the local, regional, and global patterns in marine conditions during these "non-disastrous" biotic events remains in its infancy but could provide valuable insights into the triggers and consequences of such events. Particularly, a fuller understanding of the Middle to Late Devonian marine nitrogen cycle will elucidate relationships between carbon, oxygen, and nutrient feedbacks at the time.

Herein, we report profiles of $\delta^{15}N_{bulk}$ (whole-rock $\delta^{15}N$) through the Horn River Group of the Northwest Territories, Canada, which provide information about N speciation and availability of N to primary producers of the depositional setting. The Horn River Group (latest Eifelian to Frasnian) is one of the marine stratigraphic archives dominated by laminated OM-rich mudstone, and as such, it can provide insight to oceanic biogeochemical cycling and triggers of global events which are imprinted on this interval of geologic time. These strata, which also include reef units, were deposited in the tropics, near the equator (Cocks and Torsvik, 2011; Scotese, 2014; Scotese and McKerrow, 1990) at estimated water depths of 250 to 300 m (Kabanov and Jiang, 2020), corresponding to an environment that would have been significantly impacted by the Middle to Late Devonian global events. This contribution provides an example of marine nitrogen speciation and cycling at one locality that spans a wide time range from the latest Eifelian to the late Middle or the earliest Late Frasnian, which could be compared to similar results from age-equivalent OM-rich mudstone units to assess global patterns. New and previously published $\delta^{13}C_{org}$ ($\delta^{13}C$ of OM) profiles are also included herein. Signatures of $\delta^{13}C_{org}$ from the Horn River Group have been discussed in Fraser and Hutchison (2017), Kabanov and Jiang (2020), Terlaky et al. (2020), and Kabanov et al. (2023); $\delta^{13}C_{org}$ is included in this work for comparison with $\delta^{15}N_{bulk}$ profiles.

2. Geological background

2.1. Lithostratigraphy

In the central-northern mainland Northwest Territories, the Horn River Group succession includes the Hare Indian, Ramparts, and Canol Formations, and overlies the fossiliferous limestones and calcareous mudstones of the Hume Formation carbonate platform (Fig. 1). Above the Horn River Group, the Imperial Formation comprises argillaceous mudstone and fine-grained silty sandstone (Pugh, 1983) with fossil fragments, including *Spathiocaris*, common on bedding planes (Fig. 1). Conodont age constraints for the Horn River Group and surrounding formations are presented in Fig. 1 and described in Appendix A.

The Hare Indian Formation, lowermost of the three Horn River Group units, consists of four members (Fig. 1): the Bluefish (Pugh, 1983), Bell Creek (Pyle and Gal, 2016), Francis Creek, and Prohibition Creek Members (Kabanov and Gouwy, 2017). In our study area, the Bluefish Member comprises organic-rich, calcareous to argillaceous mudstone, with intercalated fossiliferous limestone (including tentaculitids and fragments of other benthic fossils). The Francis Creek Member is characterized by organic-rich, fissile, argillaceous mudstone and is found below the siliceous to calcareous, organic-rich mudstones of the Prohibition Creek Member. In the cores studied herein, macrofossils were not observed in the Francis Creek and Prohibition Creek Members. The organic-poor mudstones of the Bell Creek Member are not present in our study area (Fig. 1).

The middle unit of the Horn River Group, the Ramparts Formation, consists of carbonate ramp, platform, and reef or bank deposits (Muir et al., 1985; Pyle and Gal, 2016), and is present only where the Bell Creek Member is thickest (Kabanov, 2019). In the cores presented in this study, the Ramparts Formation is absent (Fig. 1), and the Canol Formation overlies the Hare Indian Formation. The Canol Formation comprises two units: (1) the organic-rich, calcareous to siliceous mudstones of the Vermillion Creek Member, which occasionally contain tentaculitids, and (2) the siliceous mudstones of the Dodo Canyon Member, with a lack of macrofossils (Kabanov and Gouwy, 2017; Fig. 1).

A petrographic and geochemical study by Snowdon et al. (1987) found that the Bluefish Member and Canol Formation are dominated by Type II kerogen, derived from marine OM. Rock–Eval pyrolysis results suggest that OM in the Francis Creek and Prohibition Creek Members of the Hare Indian Formation is also primarily Type II and confirms the predominance of Type II kerogen in the Canol and Bluefish units (e.g., Pyle et al., 2014). In the Imperial Formation, Rock–Eval pyrolysis data

show that Type III (terrestrial) kerogen is present in many samples, although several samples show oxygen and hydrogen index values characteristic of primarily Type II OM (Hadlari et al., 2009).

2.2. Geological history

The Horn River Group was deposited along the northwestern margin of Laurentia (Fig. 2). Neoproterozoic supercontinental breakup was succeeded by the development of passive margins along the northwest of Laurentia, followed by convergence along the northern front (Franklinian margin) in the early Paleozoic (Dewing et al., 2019; Hadlari et al., 2014). In the study area, Early to Middle Cambrian extension and graben development (MacLean, 2011) gave way to Late Cambrian to Middle Devonian subsidence and carbonate platform development (Fritz et al., 1991; MacLean et al., 2014). From the Eifelian to the Frasnian, the study area was situated at tropical latitudes slightly to the south of the paleoequator (Fig. 2B; e.g., Cocks and Torsvik, 2011; Scotese, 2014; Scotese and McKerrow, 1990) on the paleogeographic feature known as the Mackenzie Platform (Lenz, 1972; Norris, 1985; Fig. 2), which is also referred to as the Peel Platform or Peel Shelf by some authors (e.g., Kabanov and Jiang, 2020; Morrow, 2018).

Horn River Group deposition began in the latest Eifelian with the accumulation of the OM-rich Bluefish Member of the Hare Indian Formation (Kabanov and Gouwy, 2017). The shift from Hume Formation carbonates to OM-rich mudstone deposition has been attributed to a relative sea-level rise (Gal et al., 2009; Morrow, 2018; Muir and Dixon, 1984) or to a rise in the oxygen minimum zone (Kabanov, 2019). Subsequent uplift to the northwest resulted in progradation of the Bell Creek Member mudstone banks (Muir and Dixon, 1984; Tassonyi, 1969), interpreted as marine regression (Morrow, 2018). Meanwhile, the Francis Creek and Prohibition Creek Members of the Hare Indian Formation were deposited in off-bank settings (Kabanov and Gouwy, 2017) and deposition of the Ramparts Formation carbonates began where the Bell Creek Member mudstone bank was thickest (Kabanov, 2019). The onset of another marine transgression (Morrow, 2018; Muir et al., 1985) eventually led to drowning of the Ramparts Formation carbonates and onlapping of the OM-rich Canol Formation (Muir et al., 1985; Muir and Dixon, 1984; Yose et al., 2001). In the Late Devonian, the Ellesmerian orogeny along the northern margin of Laurentia produced a foreland basin in the study area, which ended Horn River Group deposition and initiated a shift to the siliciclastic Imperial Formation (Beranek et al., 2010; Garzione et al., 1997).

Peak thermal conditions (~90 °C – 190 °C) for the Horn River Group occurred prior to the Cretaceous (Issler et al., 2005; Powell et al., 2020). This was followed by the development of a regional sub-Cretaceous unconformity caused by cooling and uplift, subsequent burial, and finally, erosion associated with the North American Cordillera foreland basin (Powell et al., 2020). Beginning in the Miocene, the study area has experienced ongoing crustal shortening, produced by accretion of the Yakutat terrane to the North American craton in the Gulf of Alaska (Mazzotti and Hyndman, 2002). The studied cores are currently situated within the eastern Laramide Cordillera, in the gently deformed hanging wall of the presently active thrust sheet of the Mackenzie Valley synclinorium (Hadlari, 2015).

2.3. Depositional conditions

The water depth of the Horn River Group depositional setting is estimated at 250–300 m (Kabanov and Jiang, 2020) and paleoclimate reconstructions for the Middle and Late Devonian predict upwelling of nutrient-rich waters along the western margin of Laurentia, particularly in the vicinity of our study area (Golonka et al., 1994). Pyle and Gal

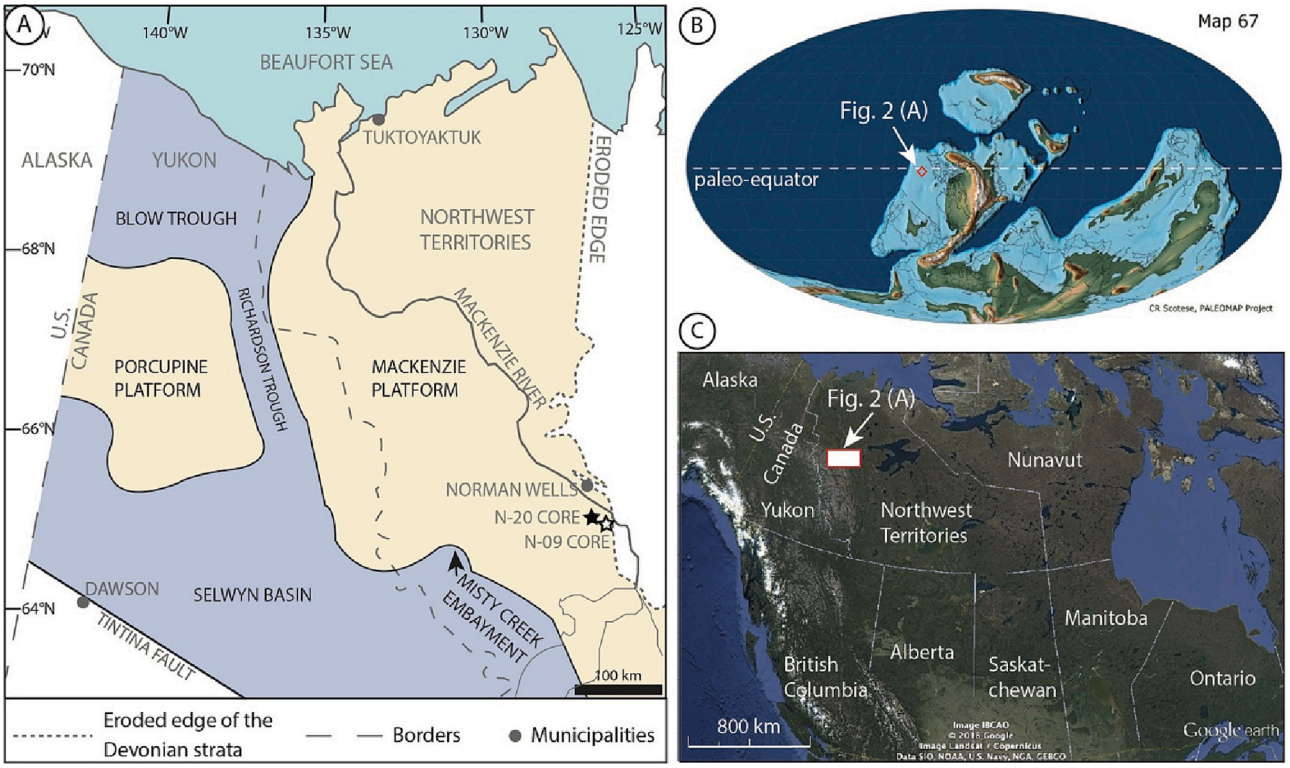

Fig. 2. Study area and paleogeography. (A) Middle to Late Devonian paleogeographic features in the northern Yukon and Northwest Territories, Canada. Grey lines and text are associated with modern-day geographic features, whereas black lines and text represent past features. The locations of the Mirror Lake N-20 and Little Bear N-09 cores are shown with black and white stars, respectively. Modified from LaGrange et al. (2022) after Pugh (1983), Al-Aasm et al. (1996) and Morrow (2018). (B) A global paleogeographic reconstruction for the Frasnian. Modified from (Scotese, 2014). (C) The position of the study area in Canada. Image modified from Google Earth Pro 7.1.8.3036 (2018). 64°58′56.91" N, 127°49′26.08" W, Eye alt 323.9 km. Data SIO, NOAA, U.S. Navy, NGA, GEBCO. (Accessed October 4, 2019).

(2016), Kabanov (2019), and Harris et al. (2021) observed enrichments of redox-sensitive trace metals (e.g., Mo, V, and U) throughout the Horn River Group and lowermost Imperial Formation, suggesting seawater or sediment anoxia at that time. For example, depending on the member, samples from the Little Bear N-09 and the Loon Creek O-06 cores showed median enrichment factors of 16–172 for Mo and 3–16 for U (Kabanov, 2019). Moreover, biomarkers for green sulfur bacteria in the Canol Formation and Bluefish Member indicate euxinia (anoxic and sulfidic conditions) within the photic zone (Kabanov and Jiang, 2020) and the Mo abundance in the Hare Indian Formation (~ 25–100 ppm) is characteristic of intermittent euxinia in the water column overlying the depositional setting (Harris et al., 2021). On the other hand, micro-scale bioturbation (< 150 μm) observed in mudstone units of the Horn River Group can only be explained by intermittent oxygenation of the seafloor, albeit perhaps mild (dysoxic conditions, 0.0–0.1 mL/L O_2; Biddle et al., 2021). The presence of spicules from glass sponges (Hexactinellida) also supports periodic weak oxygenation of bottom waters (Kabanov and Jiang, 2020). In modern sedimentary environments, these benthic sponges tolerate low dissolved oxygen and are found in water depths ranging from >500 m up to a minimum depth of 20 m; along the west coast of Canada, abundant glass sponges are currently found at water depths of 140–240 m, in a low oxygen setting (Leys et al., 2007). Although it is possible that sponge spicules were transported intrabasinally, the modern habitats of glass sponges suggest that these spicules are likely in-situ or close to.

With reference to surface water oxygenation, biomarker evidence for photic zone euxinia (Kabanov and Jiang, 2020) paired with a scarcity of macrofossils or macrofossil imprints is best explained by limited dissolved oxygen in surface waters. Supporting this assertion, pelagic microfossils, albeit with a low abundance and diversity, were observed in Horn River Group thin sections, indicating that some oxygen was present in surface waters, although limited (Biddle et al., 2021). Together, the above observations and interpretations indicate that dissolved oxygen in the water column was likely restricted to the very surface (wave-mixed) layer of the photic zone, aside from episodic instances of bottom water oxygenation.

The mechanisms that may have produced periodic bottom water oxygenation in the Horn River Group depositional environment can be distilled to three potential processes: (1) a downward shift of the upper oxygen minimum zone (OMZ) boundary, possibly caused by some high-frequency climatic periodicity comparable to ENSO (e.g., the central Peruvian Margin; Gutiérrez et al., 2008); (2) episodic bypassing of oxic ocean waters over oceanographic barriers, such as sills (e.g., the Cariaco Basin of Venezuela; Astor et al., 2003); or (3) sediment gravity flows that carry sediment and oxic waters to the depositional setting. In our study area, the presence of a hydrographic barrier similar to the Cariaco Basin has not been identified, suggesting that the Horn River Group may have been deposited in an oceanographically open system (Kabanov, 2019). Petrographic facies analysis has provided evidence for sediment-gravity-driven deposition in many intervals of the Hare Indian and Canol Formations in addition to pelagic suspension settling (Biddle et al., 2021). Considering that a topographic barrier cannot be definitively identified, the intermittent oxygenation of Horn River Group bottom waters is likely explained either by episodic sediment-gravity flows, a cyclic climatic effect, or a combination thereof.

3. Samples and analytical methods

Samples for this study were collected from two vertical cores in the Central Mackenzie Valley of the Northwest Territories, Canada (Fig. 2): (1) the ConocoPhillips Mirror Lake N-20 core located at 64°59′40.55“ N, 126°48’14.83” W (hereafter referred to as the N-20 core), and (2) the Husky Little Bear N-09 core at 64°58′55.2” N, 126°31′20.2” W (hereafter referred to as the N-09 core), which is approximately 13 km east of the N-20 core. Sample preparation methods for both cores, including de-carbonation, are summarized in Appendix A.

The N-20 core is 216.5 m long and includes the top of the Hume Formation, the entire Hare Indian and Canol Formations, and the lowermost 50 m of the Imperial Formation. Samples from this core were collected throughout the Horn River Group and the Imperial Formation at 2 m intervals except where a significant interval of core was missing. A total of 96 samples from the N-20 core were analyzed for $\delta^{13}C$ and $\delta^{15}N$ at the University of Alberta with a Thermo Scientific Delta V plus isotope ratio mass spectrometer. Both C and N isotopic results are reported using the delta notation whereby $\delta = (R_{sample}/R_{standard} - 1)$. The $\delta^{13}C_{org}$ values are reported relative to Vienna Pee Dee Belemnite (V-PDB) and the $\delta^{15}N_{bulk}$ values are reported relative to atmospheric N_2 (AIR). Two standards were used for calibration of isotopic measurements: OAS High Organic Content Sediment Standard ($\delta^{13}C = -28.9$ ‰ and $\delta^{15}N = +4.3$ ‰) and OAS Low Organic Content Soil Standard ($\delta^{13}C = -26.7$ ‰ and $\delta^{15}N = 7.0$ ‰). The analytical precision of these measurements was within 0.2 ‰ for both N and C isotopic compositions based on repeated measurements over the course of this study.

The 167.8 m N-09 core spans the uppermost Hume Formation to the lower Imperial Formation. Samples for $\delta^{13}C$ and $\delta^{15}N$ were collected at an interval of 0.6 to 0.7 m from the Bluefish Member to the lowermost Dodo Canyon Member, for a total of 144 samples. The $\delta^{13}C_{org}$ data for this core has been published by Kabanov and Jiang (2020), although the $\delta^{15}N_{bulk}$ has not previously been published. Methods for both $\delta^{13}C_{org}$ and $\delta^{15}N_{bulk}$ can be found in the supplementary materials of Kabanov and Jiang (2020) and are also summarized here. A Delta Advantage Isotope Ratio Mass Spectrometer was used for isotopic analyses. $\delta^{13}C_{org}$ values are reported relative to Vienna Pee Dee Belemnite (V-PDB) and $\delta^{15}N_{tot}$ values relative to atmospheric N_2 (AIR). Internal standards comprised: C-51 Nicotiamide ($\delta^{15}N = 0.07$, $\delta^{13}C = -22.95$), C-52 mix of ammonium sulphate and sucrose ($\delta^{15}N = 16.58$, $\delta^{13}C = -11.94$), C-54 caffeine ($\delta^{15}N = -16.61$, $\delta^{13}C = -34.46$), blind standard C-55: glutamic acid ($\delta^{15}N = -3.98$, $\delta^{13}C = -28.53$). For $\delta^{13}C$, these internal standards were calibrated to the following international standards: IAEA-CH-6 ($\delta^{13}C = -10.4$‰), NBS-22 ($\delta^{13}C = -29.91$‰), USGS-40 ($\delta^{13}C = -26.24$‰) and USGS-41 ($\delta^{13}C = 37.76$‰). For $\delta^{15}N$, the international standards IAEA-N1 ($\delta^{15}N = 0.4$‰), IAEA-N2 ($\delta^{13}C = 20.3$‰), USGS-40 ($\delta^{15}N = -4.52$‰) and USGS-41 ($\delta^{15}N = 47.57$‰) were used for calibration. Analytical precision is better than 0.2 ‰ for both nitrogen and carbon isotopic composition, based on repeated analysis of the C-55 internal standard.

A number of source rock evaluation parameters were collected by ConocoPhillips for the N-20 core and by Husky Energy for the N-09 core, some of which are included herein. From the N-09 core, these datasets include five vitrinite reflectance values and 55 total organic carbon (TOC) measurements. The N-20 core dataset comprises vitrinite and TOC for 61 samples and Oxygen Index values for 58 samples. Please see Appendix A for additional details about the methods.

4. Results

The N-09 core is characterized by a large TOC range from 1.54 wt% to 8.63 wt% (Supplementary Table 1) and a vitrinite reflectance range from 1.02% R_o to 1.29% R_o (Supplementary Table 2). The N-20 core has similar TOC range from 0.15 wt% to 7.46 wt% (Supplementary Table 1), but a larger range of vitrinite reflectance from 0.04% R_o to 1.46% R_o (Supplementary Table 2). Rock-Eval pyrolysis results and the Oxygen Index (OI) for the N-20 core can be found in Supplementary Table 3. OI, which is higher in Type III (terrestrial) kerogen than in Types I and II (Tissot and Welte, 1984), ranges from 4 to 80 mg CO_2/g C_{org} and is displayed with depth in Fig. 4. The N and C isotopic composition of samples from the N-20 core are presented in Fig. 3 and Fig. 4 and listed in Supplementary Table 4. In this core, $\delta^{13}C_{org}$ values range from −31.0 ‰ to −24.3 ‰ and $\delta^{15}N_{bulk}$ values are between −3.8 ‰ and + 1.9 ‰. For the N-09 core, $\delta^{13}C_{org}$ values are between −31.0 ‰ and − 27.2 ‰ with $\delta^{15}N_{bulk}$ values ranging from −2.0 ‰ to +5.9 ‰ (Fig. 3; Fig. 4; Supplementary Table 5).

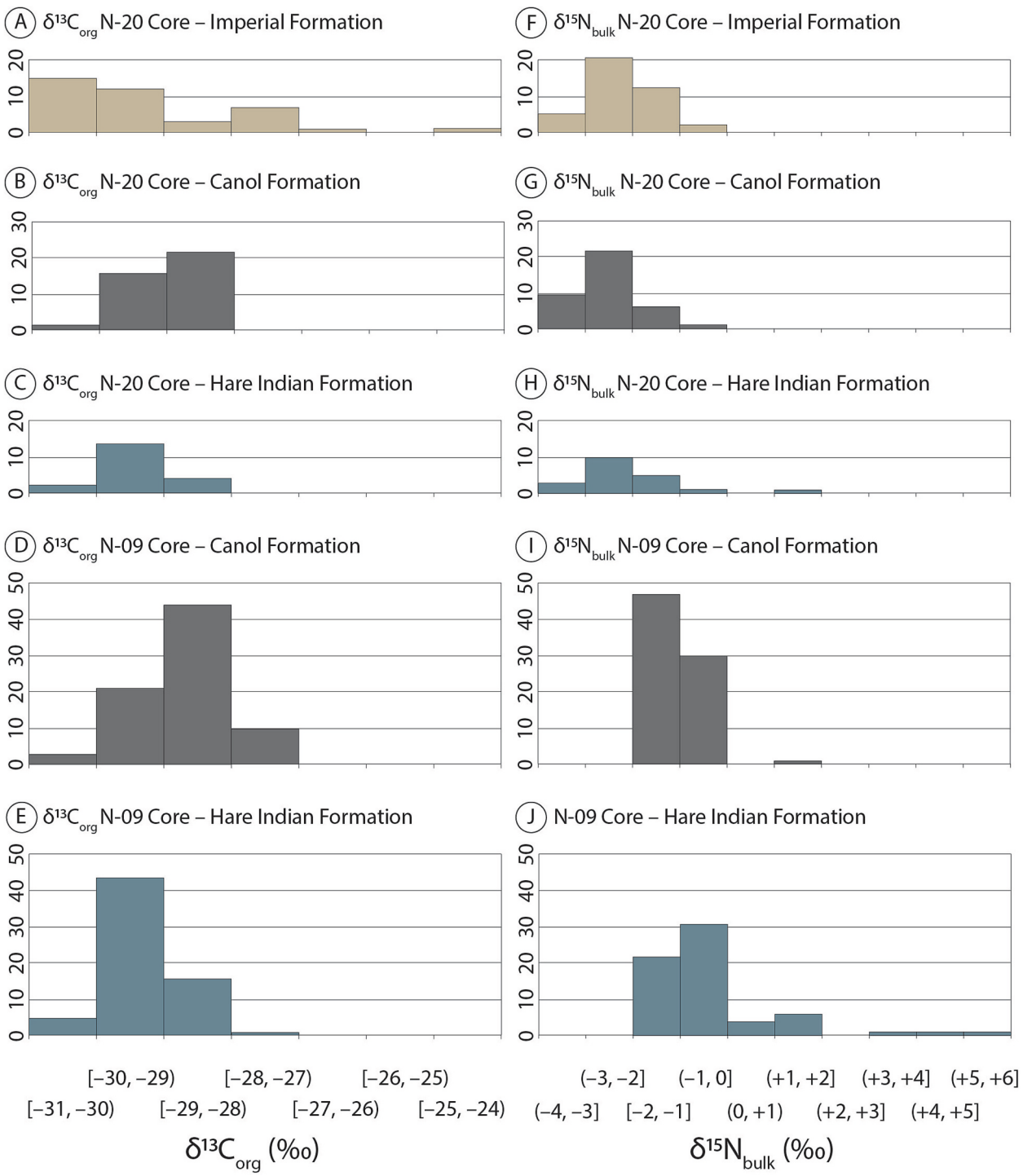

Fig. 3. Organic carbon ($\delta^{13}C_{org}$) and whole-rock nitrogen ($\delta^{15}N_{bulk}$) isotopic composition for samples from the N-20 and N-09 cores, grouped by formation.

When taken together, $\delta^{13}C_{org}$ from the N-20 and N-09 cores spans from −31.0 ‰ to −24.3 ‰ (Fig. 3). Trends in $\delta^{13}C_{org}$ are similar for both cores starting in the Bluefish Member with an initial decrease followed by an increase (Fig. 4). Following the system of Kabanov and Jiang (2020), the most notable peaks in $\delta^{13}C_{org}$ are numbered moving from the base of the cores upward (Fig. 4). First, a noticeable $\delta^{13}C_{org}$ peak (Peak A, increase of ~2 ‰) is present in the Hare Indian Formation near the Bluefish Member-Francis Creek Member contact, which is succeeded by a sharp decline throughout the Francis Creek Member. The $\delta^{13}C_{org}$ values remain relatively constant throughout the Prohibition Creek Member, after which there is an increasing trend culminating in $\delta^{13}C_{org}$ Peak B in the lower Vermillion Creek Member of the Canol Formation, representing an increase of ~1 ‰ in the N–20 core and ~ 2 ‰ in the N-09 core. The $\delta^{13}C_{org}$ values then decrease upwards throughout the Vermillion Creek Member to the contact with the Dodo Canyon Member, where Peak B2 is observed near the contact between these two members (~ 1 ‰ increase in the N-20 core and ~ 2 ‰ R increase in the N-09 core). Only the N-20 core dataset extends significantly above this contact, where the $\delta^{13}C_{org}$ values steadily decrease from Peak B2 up into the Imperial Formation, although this decline is punctuated by two spikes: Peak B3 in the Dodo Canyon Member, representing an increase of approximately 1 ‰, and the double peak of B4 and B5, which is in the

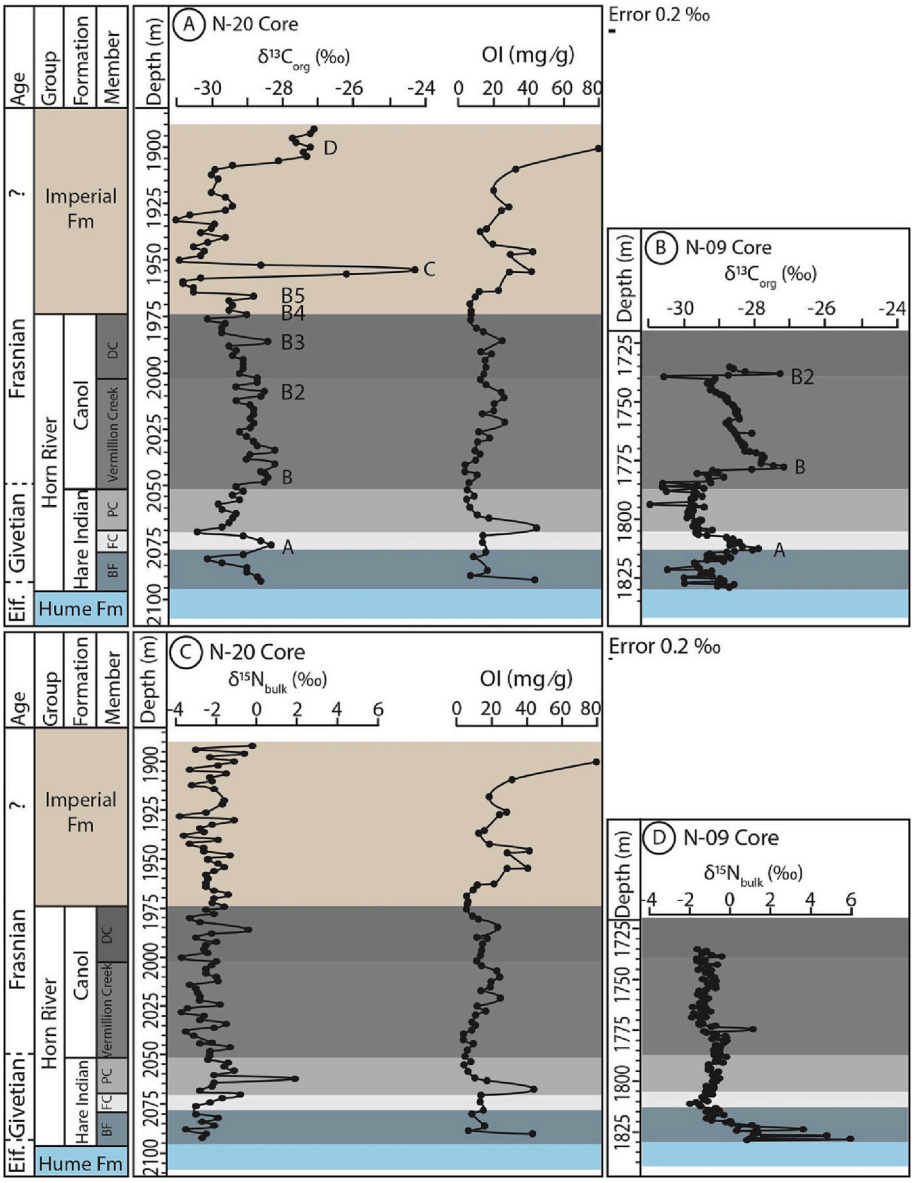

Fig. 4. Carbon isotopic composition with depth in (A) the N-20 and (B) N-09 cores. Letters label the most prominent peaks in $\delta^{13}C_{org}$. Nitrogen isotopic signatures are shown with depth in (C) the N-20 core and (D) the N-09 core. The Oxygen Index (OI) for the N-20 core is plotted for comparison with both the $\delta^{13}C_{org}$ and $\delta^{15}N_{bulk}$ profiles, with units of mg CO_2/g of organic C. Colours correspond to the members. Abbreviations: Fm – Formation, BF – Bluefish, FC – Francis Creek, PC – Prohibition Creek, and DC – Dodo Canyon. Age information for the Hare Indian and Canol Formations is based on current conodont biostratigraphy as summarized in Gouwy (2022). The exact position of the Eifelian – Givetian and the Givetian – Frasnian boundary in each core is an approximation using the available data (denoted with dashed lines). Based on the currently available biostratigraphic data, is it not possible to determine if the Frasnian to Famennian contact is present in the Imperial Formation strata of these cores.

lowermost Imperial Formation, also with an increase of about 1 ‰. The overall decrease in $\delta^{13}C_{org}$ from Peak B into the Imperial Formation is terminated by an abrupt spike (Peak C, ~ 6 ‰ increase) at 1954 m, which is followed by a shift toward heavier $\delta^{13}C_{org}$ values and another ~2 ‰ magnitude peak at approximately 1905 m (Peak D).

The $\delta^{15}N_{bulk}$ values of the N-20 core oscillate within a relatively narrow range, with most falling between −4 ‰ to 0 ‰ from the base of the core in the Bluefish Member to the top of the core in the Imperial Formation (Fig. 4; Supplementary Table 4). In the N-09 core, the $\delta^{15}N_{bulk}$ values at the base of the Bluefish Member alternate between values near 0 ‰ and heavier values ranging from approximately +3 ‰ to +6 ‰. Moving upwards in the Bluefish Member, $\delta^{15}N_{bulk}$ values decrease as they approach the overlying Francis Creek Member. From the Francis Creek Member to the Dodo Canyon Member, the $\delta^{15}N_{bulk}$ values of the N-09 core remain at relatively constant values, for the most part oscillating within a range of −2 ‰ to 0 ‰ (Fig. 4; Supplementary Table 5). Cross plots of $\delta^{13}C_{org}$ – $\delta^{15}N_{bulk}$, $\delta^{13}C_{org}$ – vitrinite, $\delta^{15}N_{bulk}$ – vitrinite, $\delta^{13}C_{org}$ – TOC, and $\delta^{15}N_{bulk}$ – TOC, details of their construction, and a discussion of their trends can be found in Appendix A.

5. Discussion

5.1. $\delta^{13}C_{org}$ Signatures

In the modern, $\delta^{13}C$ signatures of both land plants and phytoplankton vary depending on the species, within a range of approximately −20 ‰ to −30 ‰ for C_3 land plants (e.g., Fry and Sherr, 1984; Sackett, 1989; Wilson et al., 2005) and − 10 ‰ to −30 ‰ for marine phytoplankton (e.g., Falkowski, 1991; Lamb et al., 2006; Wilson et al., 2005). The $\delta^{13}C_{org}$ values from the N-20 and N-09 cores range from −31.0 ‰ to −24.3 ‰ (Fig. 4), within the approximate range for both marine phytoplankton and C_3 land plants. Microbial degradation can subsequently modify carbon isotopic signatures of OM. Studies from some areas have observed that microbial degradation does not significantly alter $\delta^{13}C$ signatures of OM (e.g., Chen et al., 2008; Galimov, 2004; Meyers and Eadie, 1993; Schelske and Hodell, 1995), whereas in other cases it has been concluded that these processes do result in small $\delta^{13}C_{org}$ shifts (e.g., Benner et al., 1987; Bottcher et al., 1998; Galimov, 2004; Lehmann et al., 2002; Prahl et al., 1997). For example, a decrease of 4 ‰ and 1.6 ‰ in $\delta^{13}C_{org}$ following microbial degradation was observed by Benner et al. (1987) and Lehmann et al. (2002),

respectively. Microbial degradation should lead to decreased $\delta^{13}C_{org}$ through enrichment of lignin in the remaining OM, which is ^{13}C poor relative to other components of OM (Benner et al., 1987; Lehmann et al., 2002). Nonetheless, these decreases may be counteracted by the in situ growth of heterotrophic microbial biomass enriched in ^{13}C compared to primary producers (Chen et al., 2008). Finally, thermal maturation of OM during burial leads to increases in $\delta^{13}C_{org}$ of the residual OM (typically by <2 ‰) because molecules with lower weight experience preferential thermal cracking (Lewan, 1983; Tang et al., 2005; Tocqué et al., 2005). Even with C isotopic shifts of a few permil associated with microbial degradation and thermal maturation (which may have counteracted one another), the $\delta^{13}C_{org}$ signatures observed are within the expected range for marine phytoplankton and C_3 plants (Falkowski, 1991; e.g., Fry and Sherr, 1984; Sackett, 1989; Wilson et al., 2005).

The $\delta^{13}C_{org}$ datasets show trends throughout the Horn River Group and overlying Imperial Formation (Fig. 4), consisting most notably of eight peaks in $\delta^{13}C_{org}$. In our dataset, $\delta^{13}C_{org}$ peaks C and D are coincident with increases in the OI profile of the N-20 core (Fig. 4). A peak in OI is also present slightly above Peak A, which is likely the product of small differences in core depth measurement between the samples taken for isotopic analysis and the samples collected by ConocoPhillips for Rock-Eval pyrolysis. The association of Peak A with a spike in OI is corroborated by the results of Kabanov and Jiang (2020), who plotted OI for the N-09 core and found an increase in OI at the same depth as Peak A. Similar to the conclusion drawn by Kabanov and Jiang (2020), our results indicate the $\delta^{13}C_{org}$ peaks A, C, and D are best explained by a larger proportion of terrestrial OM than at other depths because OI is generally higher in Type III (terrestrial OM) kerogen relative to Types I or II (Tissot and Welte, 1984). The addition of terrestrially derived OM is typically expected to also influence $\delta^{15}N_{bulk}$ signatures, which is not observed (Fig. 4). However, it is possible that temporal variations in the proportion of terrestrial OM produced shifts in $\delta^{13}C_{org}$ but not $\delta^{15}N_{bulk}$. Terrestrial plants contain a similar proportion of C as aquatic plants, but much less N (e.g., Meyers, 1994). This mass difference led Algeo et al. (2014) to suggest that the addition of a small proportion (e.g., 10–20%) of terrestrial OM has little influence on the $\delta^{15}N_{bulk}$ of the marine sedimentary units. Thus, if the fraction of terrestrial OM compared to marine OM in horizons A, C, and D is small, this would explain the absence of corresponding $\delta^{15}N_{bulk}$ shifts.

Peaks B, B2, and B3 in $\delta^{13}C_{org}$ occur in the Canol Formations, whereas peaks B4 and B5 are present at the Canol – Imperial Formations contact. Unlike peaks A, C, and D, these horizons are not associated with increases in OI. We explore the other possible causes of $\delta^{13}C_{org}$ peaks B – B5: (1) differences in thermal maturity, and (2) local changes in biological productivity and/or global changes in biological productivity associated with Devonian global events.

First, variations in the degree of thermal maturity with depth could cause trends in $\delta^{13}C_{org}$, with higher thermal maturity resulting in increased $\delta^{13}C_{org}$ (Tang et al., 2005; Tocqué et al., 2005). Average $\delta^{13}C_{org}$ and vitrinite reflectance values were cross-plotted at a two-meter interval and no relationship is observed (Supplementary Table 6; Fig. S.1). As such, it is unlikely that thermal maturation is the cause of peak B in $\delta^{13}C_{org}$.

Secondly, trends in $\delta^{13}C_{org}$ could reflect local or global scale variations in biological productivity and organic carbon burial. Biological uptake of C favours ^{12}C (Freeman, 2001) and photosynthesis in aquatic primary producers favours $CO_{2\ (aq)}$ over HCO_3^- (Degens et al., 1968). If growth rates increase, $\delta^{13}C$ values in primary producers shift toward heavier values (Falkowski, 1991; O'Leary, 1981). This heavier shift in $\delta^{13}C$ of primary producers can be explained by a switch to reliance on HCO_3^-, which is isotopically heavier, or because of a change in isotopic fractionation between dissolved inorganic C and primary producers (Hollander and McKenzie, 1991). On a larger scale, eutrophication resulting in high biological productivity is commonly proposed as a cause of Devonian global positive $\delta^{13}C$ excursions because of increased OM burial, producing depletion of ^{12}C in the marine C reservoir (e.g., Murphy et al., 2000; Pisarzowska and Racki, 2012). Thus, a spike in $\delta^{13}C_{org}$, as observed in peaks B – B5, would represent increased biological productivity, with the comparatively lower $\delta^{13}C_{org}$ values observed in between these peaks representing times of decreased production. A lack of corresponding $\delta^{15}N_{bulk}$ peaks may be explained in one of the following two ways, or a combination of both: (1) the dominant source of N was very large compared to demand by primary producers, and thus variations in primary productivity would not have resulted in variations in the degree of N isotopic fractionation, and (2) $\delta^{13}C_{org}$ peaks are the product of global-scale carbon cycle changes and do not correspond to local variations in primary productivity.

Although changes in biological productivity during deposition of the Canol Formation could have occurred on a local scale, $\delta^{13}C_{org}$ peaks B – B5 may correspond with global $\delta^{13}C$ patterns. Positive $\delta^{13}C_{carb}$ and $\delta^{13}C_{org}$ excursions have been observed and correlated in Middle to Late Devonian sedimentary intervals worldwide, many of which have been correlated with biotic crises (e.g., Lash, 2019; Zhang et al., 2019). The ultimate cause of eutrophication is debated, but high nutrient supply and elevated biological productivity is a widely accepted explanation for Devonian pulses of expanded marine anoxia (e.g., Algeo and Scheckler, 1998; Averbuch et al., 2005; Kaiho et al., 2021). Based on the Frasnian age of peaks B – B5, these may coincide with the Frasnes, Middlesex, Rhinestreet, or Kellwasser global Devonian events, all associated with known positive isotopic excursions (e.g., review in Becker et al., 2020), although, it is difficult to pinpoint without a high-resolution biostratigraphic dataset from these cores. For the N-09 and N-20 cores, Kabanov and Jiang (2020) initially speculated that $\delta^{13}C_{org}$ peaks B, B2, and B3 may coincide with the Frasnes, Middlesex, and Rhinestreet global events, respectively. However, Kabanov et al. (2023) correlated $\delta^{13}C_{org}$ and conodont results from the Prohibition Creek outcrop (ca. 30 km NE of the N-09 core) with five age-equivalent $\delta^{13}C_{org}$ profiles across Laurussia and suggested that Peak B coincides with the Frasnes event, whereas peaks B2 and B3 represent the early and late pulses of the Middlesex (*punctata*) event.

5.2. $\delta^{15}N_{bulk}$ signatures

The $\delta^{15}N_{bulk}$ values of sediments or sedimentary rocks are weighted averages of the N isotopic compositions of organic N and mineral-bound N. Because the N in detrital minerals is low and the N in authigenic minerals is mainly sourced from organic degradation, and thus has similar $\delta^{15}N$ to that of OM (Li et al., 2021; Williams et al., 1995), the $\delta^{15}N_{bulk}$ values of OM-rich sediments or sedimentary rocks are generally representative of the organic signatures of the samples. Before interpreting $\delta^{15}N_{bulk}$ values in the context of primary organic signatures, it is important to note that microbial degradation of OM during early diagenesis can produce $\delta^{15}N$ shifts. The magnitude of these changes is dependent on productivity, bottom water dissolved oxygen concentration, and sedimentation rate (Robinson et al., 2012). Accordingly, the $\delta^{15}N$ values of sediments from modern continental margin settings (shelf and slope; water depth $< \sim 1000$ m) have been found to reflect the $\delta^{15}N$ signatures of photic zone NO_3^- and sinking particles, indicating negligible early-diagenetic $\delta^{15}N$ shifts (< 2 ‰), which contrasts with deeper water, open-ocean systems typically characterized by lower productivity and sedimentation rates (Altabet et al., 1999; Freudenthal et al., 2001; Robinson et al., 2012; Thunell et al., 2004). A recent depositional interpretation of the Horn River Group points to a distal shelf setting (Biddle et al., 2021) with water depth coarsely estimated at 250–300 m (Kabanov and Jiang, 2020), which according to the modern, would have been characterized by minimal early-diagenetic $\delta^{15}N$ shifts in the sediment.

Thermal maturation is further expected to cause ^{15}N enrichment in the remaining OM as the lighter isotope is preferentially released during this process (Williams et al., 1995). Nonetheless, thermal maturation appears to have little effect on $\delta^{15}N_{bulk}$ and OM $\delta^{15}N$ values of sedimentary rocks (e.g., Boudou et al., 2008; Rivera et al., 2015), which

could be explained by retention of released N through incorporation into authigenic clay minerals as fixed NH_4^+ (Ader et al., 2016; Williams et al., 1995) or minimal N isotope fractionation during thermal N loss (Boudou et al., 2008). A cross-plot of vitrinite reflectance (a proxy for thermal maturity) and $\delta^{15}N_{bulk}$ values shows that, while the few data from the N-09 core show a rough positive trend, more data from the N-20 core clearly show no relationship between $\delta^{15}N_{bulk}$ and R_o values (Fig. S.2), suggesting that thermal maturation has not significantly affected $\delta^{15}N_{bulk}$ values in this case. Considering the potential effects of microbial degradation and thermal maturation on the $\delta^{15}N_{bulk}$ values of the Horn River Group in the N-09 and N-20 cores, we conclude that the $\delta^{15}N_{bulk}$ signatures observed are representative of the primary organic signatures of the samples.

The primary organic signature, in turn, is impacted by the type of inorganic N used by organisms that initially introduce N into the food chain. Nitrogen is first supplied to marine settings as (1) fluvial NO_3^-, with $\delta^{15}N$ values of modern riverine NO_3^- (sourced from areas with little anthropogenic fertilization) ranging from approximately −0.1 ‰ to +5 ‰ (e.g., Harrington et al., 1998; Mayer et al., 2002; Voss et al., 2006), or (2) dissolved atmospheric N_2, which has a $\delta^{15}N$ value of approximately +0.7 ‰ (Emerson et al., 1999). Processes that remove N from seawater and recycle N within the oceans can also modify the isotopic signature of the fixed N pool (primarily NO_3- and NH_4+). In OMZs of modern oceans, non-quantitative loss of fixed N through denitrification and anammox results in large $\delta^{15}N$ enrichment of the remaining NO_3^-, producing heavy $\delta^{15}N_{NO3-}$ values exceeding +15 ‰ (e.g., Brandes et al., 1998; Cline and Kaplan, 1975). However, N isotopic enrichments produced by fixed N loss are not always this large. For denitrification and anammox zones in marine sediments, models suggest positive $\delta^{15}N$ shifts in overlying water column NO_3^- that range from ~0 ‰ to +5 ‰ (e.g., Brandes and Devol, 2002; Kessler et al., 2014 and references therein) and settings characterized by water column anoxia (and thus quantitative denitrification) show very little resulting $\delta^{15}N$ enrichment of NO_3^- (e.g., Thunell et al., 2004). Nitrogen isotopic fractionation can also occur during mineralization of OM and nitrification (Ader et al., 2016), although associated shifts in $\delta^{15}N$ of the fixed N pool are minimal if these processes are near quantitative (e.g., Thunell et al., 2004).

To acquire nutrient N, some organisms assimilated fixed N, whereas other organisms, known as diazotrophs, obtain N by 'fixing' dissolved atmospheric N_2. Biological uptake of NO_3^- or NH_4^+ through assimilation can produce significant negative $\delta^{15}N$ shifts relative to the N source because the lighter ^{14}N is preferentially taken up in this process (e.g., decreases of up to ~9 ‰ for NO_3^- assimilation and up to ~25 ‰ for NH_4^+; Bauersachs et al., 2009; Pennock et al., 1996). The degree of fractionation depends on the availability of fixed N and the biological growth rate, with higher N availability and/or lower growth rates associated with higher fractionation and thus lighter $\delta^{15}N$ in primary producers (e.g., Hoch et al., 1994; Kessler et al., 2014; Thunell et al., 2004; Wada et al., 1990). Studies of modern diazotrophic cyanobacteria have shown that fractionation during N_2 fixation catalyzed by Mo (the most common catalyst in modern oceans) varies from ~ −2 ‰ to −3 ‰, resulting in biomass $\delta^{15}N$ values of −2 ‰ to 0 ‰ (e.g., Bauersachs et al., 2009; Carpenter et al., 1997; Minagawa and Wada, 1986; Montoya et al., 2002).

In our samples, the $\delta^{15}N_{bulk}$ values are mostly between 0 ‰ and − 4 ‰ in the N-20 core and 0 ‰ and − 2 ‰ in the N-09 core (except for the Bluefish Member, which will be discussed below). These persistent negative $\delta^{15}N_{bulk}$ values could be obtained in one or more of the following ways: (1) assimilation of abundant (non-limiting) NO_3^-, (2) N_2 fixation, or (3) assimilation of abundant (non-limiting) NH_4^+. First, NO_3^- assimilation from a NO_3^--unlimited reservoir is associated with a large isotopic effect and can result in a similar $\delta^{15}N$ range to the values observed in this study (Bauersachs et al., 2009). We discount this first possibility; it is unlikely that NO_3^- was abundant to the point that it was non-limiting for growth considering the interpreted paleoredox conditions (regularly occurring photic zone euxinia). Second, the low $\delta^{15}N_{bulk}$ values in our samples could be the product of N_2 fixation. Although paleoredox conditions would have limited the presence of aerobic diazotrophs (e.g., the cyanobacteria *Trichodesmium*) to the uppermost oxygenated water column, anaerobic diazotrophs (e.g., the bacteria *Vibrio diazotrophicus*) could have occupied the deeper shelfal waters, much like in the modern, including the Costa Rica Dome OMZ (Cheung et al., 2016) and the Peru Margin OMZ (e.g., Loescher et al., 2014). Finally, abundant NH_4^+ could lead to N isotopic fractionation during assimilation, producing ^{15}N-depleted biomass (e.g., Ader et al., 2016; Higgins et al., 2012; Junium and Arthur, 2007; Uveges et al., 2020) and $\delta^{15}N$ values similar to those seen herein. A scenario of abundant NH_4^+ is plausible for the Horn River Group given that highly reducing conditions in the water column would have been associated with low levels of nitrification. Moreover, biomarker evidence for photic zone euxinia (Kabanov and Jiang, 2020) implies that NH_4^+ would have been available to primary producers. Overall, the paleoredox regime of our depositional setting likely allowed for both N_2-fixation and NH_4^+ assimilation, similar to the processes proposed by Higgins et al. (2012) for the Cenomanian– Turonian Ocean Anoxic Event (OAE 2) at the Demerara Rise.

Nonetheless, it is important to note that a comparison of $\delta^{15}N_{bulk}$ to $\delta^{13}C_{org}$ does not show any relationship (Fig. S.3). This suggests a decoupling of the sources or processes that affect C and N in strata of N-20 and N-09 cores. If phytoplankton used C and N both from dissolved ions, the $\delta^{13}C_{org}$ and $\delta^{15}N_{bulk}$ values should vary parallelly as primary productivity changes, but this covariance is not observed, which suggests that primary producers instead derived N from atmospheric N_2 (e.g., Hodell and Schelske, 1998; Li et al., 2008). Interestingly, biomarker results point to the presence of green sulfur bacteria (anaerobic phototrophs) in the Bluefish Member of the Hare Indian Formation and the Canol Formation (Kabanov and Jiang, 2020) and many modern species of these bacteria are diazotrophic (e.g., Madigan, 1995). In sum, although it is plausible that a certain degree of NH_4^+ assimilation occurred, the lack of $\delta^{15}N_{bulk} - \delta^{13}C_{org}$ relationships suggests that N_2 was the dominant N species used by primary producers.

The $\delta^{15}N_{bulk}$ values of the N-09 core show a peak in the Bluefish Member near the contact with the underlying Hume Formation (Fig. 4). This contact represents drowning of the underlying carbonate platform caused by marine transgression (Morrow, 2018), also interpreted as a drowning unconformity sensu W. Schlager (Kabanov and Gouwy, 2017). In the N-09 core, the interval at the base of the Bluefish Member is characterized by OM-rich, calcareous to argillaceous mudstone intercalated with limestone laminae and beds, which are commonly graded, and contain tentaculitids and fragments of other benthic fossils such as *Amphipora*, brachiopods, and ostracods (Kabanov et al., 2016). These characteristics of the limestone beds suggest that they comprise transported debris, possibly derived from an up-dip area where the carbonate factory was still operating following significant relative sea-level rise. The relatively high $\delta^{15}N_{bulk}$ values observed at the base of the Bluefish Member in the N-09 core likely correspond to these limestone beds. OM with higher $\delta^{15}N$ was likely transported along with carbonate debris from a more proximal area where higher dissolved oxygen in the water column meant that NO_3^- was available to primary producers. The absence of similarly high $\delta^{15}N$ readings in the N-20 core can be explained by two factors. First, in the N-09 core, the stratigraphically lowest sample was collected right at the Bluefish Member – Hume Formation contact, whereas the lowest sample from the N-20 core was collected 2.9 m above the Bluefish Member base. Secondly, the sampling spacing for the N-20 core (2 m) was somewhat coarser than for the N-09 core (0.6–0.7 m), making it more likely that the basal Bluefish limestone beds comprising transported debris were not sampled.

Aside from the high $\delta^{15}N_{bulk}$ values at the base of the N-09 core Bluefish Member, the $\delta^{15}N_{bulk}$ oscillations observed throughout the length of both cores (Fig. 4) may be the product of the episodic weak oxygenation events that characterized the depositional setting. For example, in Lake Kivu (Eastern Africa), Uveges et al. (2020) observed that mixing events, which supplied oxygen to anoxic deep waters,

ultimately gave rise to spikes in sediment $\delta^{15}N_{bulk}$ through an increase in water-column denitrification and anammox. Non-quantitative denitrification and anammox, as expected in weakly oxygenated conditions, result in ^{15}N enrichment of the remaining fixed N pool (e.g., Brandes et al., 1998; Cline and Kaplan, 1975), which could increase $\delta^{15}N$ of biomass through biological assimilation of the isotopically enriched N species. Compared to modern sediments, Uveges et al. (2020) suggested that $\delta^{15}N_{bulk}$ fluctuations produced by oxygenation events are expected to be muted in organic-rich mudstone units because of sediment compaction and time-averaging. The oscillations in our $\delta^{15}N_{bulk}$ dataset likely serve as an example of one such muted record of episodic and relatively brief disturbances to the background paleoredox state.

Finally, relative to the N-09 core, the $\delta^{15}N_{bulk}$ signatures from the N-20 core are on average 1.4 ‰ lower in the Canol Formation and 1.6 ‰ lower in the Hare Indian Formation (Figs. 3 and 4; Supplementary Tables 4 and 5). Although a small inter-lab $\delta^{15}N$ discrepancy could occur, these large differences in $\delta^{15}N_{bulk}$ are more likely explained by somewhat differing marine conditions at the location of each core. The N-20 core is situated approximately 13 km to the WNW from the N-09 core and thus was deposited in a seaward position. It is possible that there were differences in the supply of nutrients or abundance of oxygen in surface waters between these two positions in the basin, affecting the abundance of fixed N. If this difference were instead attributed to contrasting burial depth and thermal maturity between the two cores, this would mean that the N-09 core experienced a higher thermal degradation of OM than the N-20 core. In fact, vitrinite reflectance values from the two cores are comparable (Fig. S.1) and the N-20 was buried deeper, which discounts the possibility of variations in thermal maturity as the cause of the $\delta^{15}N_{bulk}$ differences.

6. Conclusions

A high-resolution dataset comprising $\delta^{15}N_{bulk}$ and $\delta^{13}C_{org}$ was collected from OM-rich mudstone samples of the Middle to Late Devonian Horn River at two locations in the Central Mackenzie Valley of the Northwest Territories, Canada. Vitrinite reflectance, TOC, and Rock-Eval pyrolysis datasets were integrated with the $\delta^{15}N_{bulk}$ and $\delta^{13}C_{org}$ to provide information about thermal maturity and OM type and abundance. The following key conclusions are drawn from our results:

- $\delta^{15}N_{bulk}$ values ranging from −4 ‰ to 0 ‰ and a lack of $\delta^{15}N_{bulk}$ – $\delta^{13}C_{org}$ relationship suggest that dissolved N_2 was the primary N species used by primary producers.
- Regular oscillations in the $\delta^{15}N_{bulk}$ dataset likely represent a muted record of high frequency but relatively brief episodes of mild oxygenation that punctuate a background state of photic zone euxinia at this location.
- Spikes in $\delta^{13}C_{org}$ are not accompanied by corresponding changes in $\delta^{15}N_{bulk}$. In particular, $\delta^{13}C_{org}$ peaks in the Canol Formation, which have been interpreted by other authors as representing global Devonian events, do not show matching changes in $\delta^{15}N_{bulk}$. These results suggest that nutrient N speciation and nutrient N cycling processes remained relatively constant at this location, despite the global scale changes in the marine realm that characterize the Middle to Late Devonian period of Earth's history.

Correlations of this $\delta^{15}N_{bulk}$ record from northwest Canada with $\delta^{15}N_{bulk}$ datasets from age-equivalent organic-rich mudstone units are suggested as important next steps. Such comparisons will contribute to a clearer picture of the regional and global N cycle during the Middle to Late Devonian, a time characterized by successive marine biotic crises and widespread deposition of organic-rich mudstone.

Declaration of Competing Interest

The authors declare that they have no known competing financial interests or personal relationships that could have appeared to influence the work reported in this paper.

Data availability

The dataset for this article is included as supplementary tables.

Acknowledgments

We are grateful to the Northwest Territories Geological Survey and to the GSA (GSA Graduate Student Research Grant no. **13266-21)** for funding of this work. Additionally, we would like to thank Rizal Ignacio and Marcus Kehler for help with sample preparation. Geological Survey of Canada (GSC) data used in this paper were obtained through the Geomapping for Energy and Minerals (GEM) program of NRCan; it is NRCan contribution no. 20220353.

Appendix A. Supplementary data

Supplementary data to this article can be found online at https://doi.org/10.1016/j.palaeo.2023.111512.

References

Ader, M., Thomazo, C., Sansjofre, P., Busigny, V., Papineau, D., Laffont, R., Cartigny, P., Halverson, G.P., 2016. Interpretation of the nitrogen isotopic composition of Precambrian sedimentary rocks: assumptions and perspectives. Chem. Geol. 429, 93–110. https://doi.org/10.1016/j.chemgeo.2016.02.010.

Al-Aasm, I.S., Morad, S., Durocher, S., Muir, I., 1996. Sedimentology, C-S–Fe relationships and stable isotopic compositions in Devonian black mudrocks, Mackenzie Mountains, Northwest Territories,Canada. Sediment. Geol. 106, 279–298. https://doi.org/10.1016/S0037-0738(96)00018-8.

Algeo, T.J., Meyers, P.A., Robinson, R.S., Rowe, H., Jiang, G.Q., 2014. Icehouse–greenhouse variations in marine denitrification. Biogeosciences 11, 1273–1295. https://doi.org/10.5194/bg-11-1273-2014.

Algeo, T.J., Scheckler, S.E., 1998. Terrestrial-marine teleconnections in the Devonian: links between the evolution of land plants, weathering processes, and marine anoxic events. Philos. Trans. R. Soc. Lond. Ser. B Biol. Sci. 353, 113–130. https://doi.org/10.1098/rstb.1998.0195.

Altabet, M.A., Pilskaln, C., Thunell, R., Pride, C., Sigman, D., Chavez, F., Francois, R., 1999. The nitrogen isotope biogeochemistry of sinking particles from the margin of the Eastern North Pacific. Deep Sea ResPart Oceanogr. Res. Pap. 46, 655–679. https://doi.org/10.1016/S0967-0637(98)00084-3.

Astor, Y., Muller-Karger, F., Scranton, M.I., 2003. Seasonal and interannual variation in the hydrography of the Cariaco Basin: implications for basin ventilation. Cont. Shelf Res. 23, 125–144. https://doi.org/10.1016/S0278-4343(02)00130-9.

Averbuch, O., Tribovillard, N., Devleeschouwer, X., Riquier, L., Mistiaen, B., Van Vliet-Lanoe, B., 2005. Mountain building-enhanced continental weathering and organic carbon burial as major causes for climatic cooling at the Frasnian-Famennian boundary (c. 376 Ma)? Terra Nova 17, 25–34. https://doi.org/10.1111/j.1365-3121.2004.00580.x.

Bauersachs, T., Schouten, S., Compaoré, J., Wollenzien, U., Stal, L.J., Sinninghe Damsteé, J.S., 2009. Nitrogen isotopic fractionation associated with growth on dinitrogen gas and nitrate by cyanobacteria. Limnol. Oceanogr. 54, 1403–1411. https://doi.org/10.4319/lo.2009.54.4.1403.

Becker, R.T., Marshall, J.E.A., Da Silva, A.-C., Agterberg, F.P., Gradstein, F.M., Ogg, J.G., 2020. Chapter 22 - The Devonian Period. In: Gradstein, Felix M., Ogg, James G., Schmitz, M.D., Ogg, G.M. (Eds.), Geologic Time Scale 2020. Elsevier, pp. 733–810. https://doi.org/10.1016/B978-0-12-824360-2.00022-X.

Benner, R., Fogel, M.L., Sprague, E.K., Hodson, R.E., 1987. Depletion of 13C in lignin and its implications for stable carbon isotope studies. Nature 329, 708–710. https://doi.org/10.1038/329708a0.

Beranek, L.P., Mortensen, J.K., Lane, L.S., Allen, T.L., Fraser, T.A., Hadlari, T., Zantvoort, W.G., 2010. Detrital zircon geochronology of the western Ellesmerian clastic wedge, northwestern Canada: insights on Arctic tectonics and the evolution of the northern Cordilleran miogeocline. GSA Bull. 122, 1899–1911. https://doi.org/10.1130/B30120.1.

Biddle, S.K., LaGrange, M.T., Harris, B.S., Fiess, K., Terlaky, V., Gingras, M.K., 2021. A fine detail physico-chemical depositional model for Devonian organic-rich mudstones: a petrographic study of the Hare indian and Canol Formations, Central Mackenzie Valley,Northwest Territories. Sediment. Geol. 414, 105838 https://doi.org/10.1016/j.sedgeo.2020.105838.

Bottcher, M.E., Oelschlager, B., Hopner, T., Brumsack, H.-J., Rullkotter, J., 1998. Sulfate reduction related to the early diagenetic degradation of organic matter and "black spot" formation in tidal sandflats of the German Wadden Sea (southern North Sea): stable isotope (13C, 34S, 18O) and other geochemical results. Org. Geochem. 29, 1517–1530.

Boudou, J.-P., Schimmelmann, A., Ader, M., Mastalerz, M., Sebilo, M., Gengembre, L., 2008. Organic nitrogen chemistry during low-grade metamorphism. Geochim. Cosmochim. Acta 72, 1199–1221. https://doi.org/10.1016/j.gca.2007.12.004.

Brandes, J.A., Devol, A.H., 2002. A global marine-fixed nitrogen isotopic budget: implications for Holocene nitrogen cycling. Glob. Biogeochem. Cycles 16. https://doi.org/10.1029/2001GB001856, 67–1-67–14.

Brandes, J.A., Devol, A.H., Yoshinari, T., Jayakumar, D.A., Naqvi, S.W.A., 1998. Isotopic composition of nitrate in the central Arabian Sea and eastern tropical North Pacific: a tracer for mixing and nitrogen cycles. Limnol. Oceanogr. 43, 1680–1689. https://doi.org/10.4319/lo.1998.43.7.1680.

Carmichael, S.K., Waters, J.A., Königshof, P., Suttner, T.J., Kido, E., 2019. Paleogeography and paleoenvironments of the Late Devonian Kellwasser event: a review of its sedimentological and geochemical expression. Glob. Planet. Change 183, 102984. https://doi.org/10.1016/j.gloplacha.2019.102984.

Carpenter, E.J., Harvey, H.R., Fry, B., Capone, D.G., 1997. Biogeochemical tracers of the marine cyanobacterium Trichodesmium. Deep Sea ResPart Oceanogr. Res. Pap. 44, 27–38. https://doi.org/10.1016/S0967-0637(96)00091-X.

Chen, F., Zhang, L., Yang, Y., Zhang, D., 2008. Chemical and isotopic alteration of organic matter during early diagenesis: evidence from the coastal area off-shore the Pearl River estuary, South China. J. Mar. Syst. 74, 372–380. https://doi.org/10.1016/j.jmarsys.2008.02.004.

Cheung, S., Xia, X., Guo, C., Liu, H., 2016. Diazotroph community structure in the deep oxygen minimum zone of the Costa Rica Dome. J. Plankton Res. 38, 380–391. https://doi.org/10.1093/plankt/fbw003.

Cline, J.D., Kaplan, I.R., 1975. Isotopic fractionation of dissolved nitrate during denitrification in the eastern tropical North Pacific Ocean. Mar. Chem. 3, 271–299. https://doi.org/10.1016/0304-4203(75)90009-2.

Cocks, L.R.M., Torsvik, T.H., 2011. The Palaeozoic geography of Laurentia and western Laurussia: a stable craton with mobile margins. Earth-Sci. Rev. 106, 1–51. https://doi.org/10.1016/j.earscirev.2011.01.007.

Copper, P., 2002. Silurian and Devonian Reefs: 80 Million Years of Global Greenhouse Between Two Ice Ages.

Degens, E.T., Gullard, R.R., Sackett, W.M., Hellebust, J.A., 1968. Metabolic fractionation of carbon isotopes in marine plankton: 1. Temperature and respiration experiments. Deep-Sea Res. 15, 1–9. https://doi.org/10.1016/0011-7471(68)90024-7.

Dewing, K., Hadlari, T., Pearson, D.G., Matthews, W., 2019. Early Ordovician to Early Devonian tectonic development of the northern margin of Laurentia,Canadian Arctic Islands. GSA Bull. 131, 1075–1094. https://doi.org/10.1130/B35017.1.

Emerson, S., Stump, C., Wilbur, D., Quay, P., 1999. Accurate measurement of O2, N2, and Ar gases in water and the solubility of N2. Mar. Chem. 64, 337–347. https://doi.org/10.1016/S0304-4203(98)00090-5.

Falkowski, P.G., 1991. Species variability in the fractionation of 13C and 12C by marine phytoplankton. J. Phytoplankton Res. 13, 21–28.

Fraser, T.A., Hutchison, M.P., 2017. Lithogeochemical characterization of the Middle-Upper Devonian Road River Group and Canol and Imperial formations on Trail River, East Richardson Mountains, Yukon: age constraints and a depositional model for fine-grained strata in the lower Paleozoic Richardson trough. Can. J. Earth Sci. 54, 731–765. https://doi.org/10.1139/cjes-2016-0216.

Freeman, K.H., 2001. Isotopic biogeochemistry of marine organic carbon. Rev. Mineral. Geochem. 43, 579–605. https://doi.org/10.2138/gsrmg.43.1.579.

Freudenthal, T., Wagner, T., Wenzhöfer, F., Zabel, M., Wefer, G., 2001. Early diagenesis of organic matter from sediments of the eastern subtropical Atlantic: evidence from stable nitrogen and carbon isotopes. Geochim. Cosmochim. Acta 65, 1795–1808. https://doi.org/10.1016/S0016-7037(01)00554-3.

Fritz, W.H., Cecile, M.P., Norford, B.S., Morrow, D., Geldsetzer, H.H.J., 1991. Cambrian to Middle Devonian assemblages. In: Geology of the Cordilleran Orogen in Canada. Geological Society of America. https://doi.org/10.1130/DNAG-GNA-G2.151.

Fry, B., Sherr, E.B., 1984. δ13C measurements as indicators of carbon flow in marine and freshwater ecosystems. Contrib. Mar. Sci. 27, 13–47.

Gal, L.P., Pyle, L.J., Hadlari, T., Allen, T.L., 2009. Chapter 6: Lower to Upper Devonian strata, Arnica-Landry play, and Kee Scarp play. In: Pyle, L.J., Jones, A. (Eds.), Regional Geoscience Studies and Petroleum Potential, Peel Plateau and Plain, Northwest Territories and Yukon: Project Volume, Northwest Territories Geoscience Office and Yukon Geological Survey, NWT, Open File 2009-002 and Yukon Geological Survey Open File 2009-25.

Galimov, E.M., 2004. The pattern of δ13Corg versus HI/OI relation in recent sediments as an indicator of geochemical regime in marine basins: comparison of the Black Sea, Kara Sea, and Cariaco Trench. Chem. Geol. 204, 287–301. https://doi.org/10.1016/j.chemgeo.2003.11.014.

Garzione, C.N., Patchett, P.J., Ross, G.M., Nelson, J., 1997. Provenance of Paleozoic sedimentary rocks in the Canadian Cordilleran miogeocline: a Nd isotopic study. Can. J. Earth Sci. 34, 1603–1618. https://doi.org/10.1139/e17-129.

Golonka, J., Ross, M.I., Scotese, C.R., 1994. Phanerozoic Paleogeographic and Paleoclimatic Modeling Maps 1–47.

Gouwy, S.A., 2022. Devonian conodont biostratigraphy of the Mackenzie Mountains, western part of the Northwest Territories. In: Lavoie, D., Dewing, K. (Eds.), Sedimentary Basins of Northern Canada: Contributions to a 1000 Ma Geological Journey and Insight on Resource Potential, Geological Survey of Canada Bulletin 609.

Gutiérrez, D., Enríquez, E., Purca, S., Quipúzcoa, L., Marquina, R., Flores, G., Graco, M., 2008. Oxygenation episodes on the continental shelf of Central Peru: remote forcing and benthic ecosystem response. Prog. Oceanogr. 79, 177–189. https://doi.org/10.1016/j.pocean.2008.10.025.

Hadlari, T., 2015. Oil migration driven by exhumation of the Canol Formation oil shale: a new conceptual model for the Norman Wells oil field, northwestern Canada. Mar. Pet. Geol. 65, 172–177. https://doi.org/10.1016/j.marpetgeo.2015.03.027.

Hadlari, T., Davis, W.J., Dewing, K., 2014. A pericratonic model for the Pearya terrane as an extension of the Franklinian margin of Laurentia, Canadian Arctic. Geol. Soc. Am. Bull. 126, 182–200. https://doi.org/10.1130/B30843.1.

Hadlari, T., Gal, L.P., Zantvoort, W.G., Tylosky, S.A., Allen, T.L., Fraser, T.A., Lemieux, Y., Catuneanu, O., 2009. Chapter 7 – Upper Devonian to Carboniferous Strata I - Imperial Formation Play. In: Pyle, L.J., Jones, A.L. (Eds.), Regional Geoscience Studies and Petroleum Potential of Peel Plateau and Plain, Northwest Territories and Yukon: Project Volume, Northwest Territories Geoscience Office and Yukon Geological Survey, NWT Open File 2009-02 and YGS Open File 2009-25, pp. 290–364.

Harrington, R.R., Kennedy, B.P., Chamberlain, C.P., Blum, J.D., Folt, C.L., 1998. 15N enrichment in agricultural catchments: field patterns and applications to tracking Atlantic salmon (Salmo salar). Chem. Geol. 147, 281–294. https://doi.org/10.1016/S0009-2541(98)00018-7.

Harris, B.S., LaGrange, M.T., Biddle, S.K., Playter, T.L., Fiess, K.M., Gingras, M.K., 2021. Chemostratigraphy as a tool for sequence stratigraphy in the Devonian Hare Indian Formation in the Mackenzie Mountains and Central Mackenzie Valley, Northwest Territories,Canada. Can. J. Earth Sci. 99, 1–17.

Higgins, M.B., Robinson, R.S., Husson, J.M., Carter, S., Pearson, A., 2012. In: Dominant eukaryotic export production during ocean anoxic events reflects the importance of recycled NH4+ 109, pp. 2269–2274. https://doi.org/10.1073/pnas.1104313109.

Hoch, M.P., Fogel, M.L., Kirchman, D.L., 1994. Isotope fractionation during ammonium uptake by marine microbial assemblages. Geomicrobiol J. 12, 113–127. https://doi.org/10.1080/01490459409377977.

Hodell, D.A., Schelske, C.L., 1998. Production, sedimentation, and isotopic composition of organic matter in Lake Ontario. Limnol. Oceanogr. 43 (2), 200–214.

Hollander, D.J., McKenzie, J.A., 1991. CO2 control on carbon-isotope fractionation during aqueous photosynthesis: A paleo-pCO2 barometer. Geology 19 (9), 929–932.

House, M.R., 1985. Correlation of mid-Palaeozoic ammonoid evolutionary events with global sedimentary perturbations. Nature 313, 17–22. https://doi.org/10.1038/313017a0.

Issler, D.R., Grist, A.M., Stasiuk, L.D., 2005. Post-Early Devonian thermal constraints on hydrocarbon source rock maturation in the Keele Tectonic Zone, Tulita area, NWT, Canada, from multi-kinetic apatite fission track thermochronology, vitrinite reflectance and shale compaction. Bull. Can. Pet. Geol. 53, 405–431. https://doi.org/10.2113/53.4.405.

Junium, C.K., Arthur, M.A., 2007. Nitrogen cycling during the Cretaceous, Cenomanian-Turonian Oceanic Anoxic Event II. Geochem. Geophys. Geosystems 8. https://doi.org/10.1029/2006GC001328.

Kabanov, P., 2019. Devonian (c. 388–375 Ma) Horn River Group of Mackenzie Platform (NW Canada) is an open-shelf succession recording oceanic anoxic events. J. Geol. Soc. 176, 29–45. https://doi.org/10.1144/jgs2018-075.

Kabanov, P., Deblonde, C., 2019. Geological and geochemical data from Mackenzie Corridor. Part VIII: Middle-Upper Devonian lithostratigraphy, formation tops, and isopach maps in NTS areas 96 and 106, Northwest Territories and Yukon (Geological Survey of Canada Open File Report No. 8552). https://doi.org/10.4095/314785.

Kabanov, P., Gouwy, S., Lawrence, P.A., Weleschuk, D.J., Chan, W.C., 2016. Geological and geochemical data from Mackenzie Corridor. Part III: New data on lithofacies, micropaleontology, lithogeochemistry, and Rock-EvalTM pyrolysis from the Devonian Horn River Group in the Mackenzie Plain and Norman Range, Northwest Territories (Geological Survey of Canada Open File Report No. 7951).

Kabanov, P., Gouwy, S.A., 2017. The Devonian Horn River Group and the basal Imperial Formation of the central Mackenzie Plain, N.W.T., Canada: multiproxy stratigraphic framework of a black shale basin. Can. J. Earth Sci. 54, 409–429. https://doi.org/10.1139/cjes-2016-0096.

Kabanov, P., Gouwy, S.A., van der Boon, A., Grasby, S.E., 2023. Nature of Devonian Anoxic events based on multiproxy records from Panthalassa, Nw Canada [Manuscript submitted for publication].

Kabanov, P., Jiang, C., 2020. Photic-zone euxinia and anoxic events in a Middle-Late Devonian shelfal sea of Panthalassan continental margin, NW Canada: changing paradigm of Devonian Ocean and sea level fluctuations. Glob. Planet. Change 188, 103153. https://doi.org/10.1016/j.gloplacha.2020.103153.

Kaiho, K., Miura, M., Tezuka, M., Hayashi, N., Jones, D.S., Oikawa, K., Casier, J.-G., Fujibayashi, M., Chen, Z.-Q., 2021. Coronene, mercury, and biomarker data support a link between extinction magnitude and volcanic intensity in the Late Devonian. Glob. Planet. Change 199, 103452. https://doi.org/10.1016/j.gloplacha.2021.103452.

Kessler, A.J., Bristow, L.A., Cardenas, M.B., Glud, R.N., Thamdrup, B., Cook, P.L.M., 2014. The isotope effect of denitrification in permeable sediments. Geochim. Cosmochim. Acta 133, 156–167. https://doi.org/10.1016/j.gca.2014.02.029.

Klemme, H.D., Ulmishek, G.F., 1991. Effective petroleum source rocks of the world: stratigraphic distribution and controlling depositional factors. Am. Assoc. Pet. Geol. Bull. 75, 1809–1851. https://doi.org/10.1306/0C9B2A47-1710-11D7-8645000102C1865D.

LaGrange, M.T., Atienza, N.M.M., Biddle, S.K., Harris, B.S., Fiess, K.M., Terlaky, V., Konhauser, K.O., Gingras, M.K., 2022. The nature, origin, and predictors of porosity in the Middle to Late Devonian Horn River Group of the Central Mackenzie Valley, Northwest TerritoriesCanada. Mar. Pet. Geol. 142, 105738 https://doi.org/10.1016/j.marpetgeo.2022.105738.

Lamb, A.L., Wilson, G.P., Leng, M.J., 2006. A review of coastal palaeoclimate and relative sea-level reconstructions using δ13C and C/N ratios in organic material. Earth-Sci. Rev. 75, 29–57. https://doi.org/10.1016/j.earscirev.2005.10.003.

Lash, G.G., 2019. A global biogeochemical perturbation during the Middle Frasnian punctata event: evidence from muted carbon isotope signature in the Appalachian Basin, New York State (USA). Glob. Planet. Change 177, 239–254. https://doi.org/10.1016/j.gloplacha.2019.01.006.

Lehmann, M.F., Bernasconi, S.M., Barbieri, A., McKenzie, J.A., 2002. Preservation of organic matter and alteration of its carbon and nitrogen isotope composition during simulated and in situ early sedimentary diagenesis. Geochim. Cosmochim. Acta 66, 3573–3584. https://doi.org/10.1016/S0016-7037(02)00968-7.

Lenz, A.C., 1972. Ordovician to Devonian history of northern Yukon and adjacent district of Mackenzie. Bull. Can. Petrol. Geol. 20, 321–361. https://doi.org/10.35767/gscpgbull.20.2.321.

Lewan, M.D., 1983. Effects of thermal maturation on stable organic carbon isotopes as determined by hydrous pyrolysis of Woodford Shale. Geochim. Cosmochim. Acta 47, 1471–1479. https://doi.org/10.1016/0016-7037(83)90306-X.

Leys, S.P., Mackie, G.O., Reiswig, H.M., 2007. The biology of glass sponges. In: Advances in Marine Biology. Academic Press, pp. 1–145. https://doi.org/10.1016/S0065-2881(06)52001-2.

Li, Y., Li, L., Wu, Z., 2021. First-principles calculations of equilibrium nitrogen isotope fractionations among aqueous ammonium, silicate minerals and salts. Geochim. Cosmochim. Acta 297, 220–232. https://doi.org/10.1016/j.gca.2021.01.019.

Li, L., Yu, Z., Moeller, R.E., Bebout, G.E., 2008. Complex trajectories of aquatic and terrestrial ecosystem shifts caused by multiple human-induced environmental stresses. Geochimica et Cosmochimica Acta 72 (17), 4338–4351.

Loescher, C.R., Großkopf, T., Desai, F.D., Gill, D., Schunck, H., Croot, P.L., Schlosser, C., Neulinger, S.C., Pinnow, N., Lavik, G., Kuypers, M.M.M., LaRoche, J., Schmitz, R.A., 2014. Facets of diazotrophy in the oxygen minimum zone waters off Peru. ISME J. 8, 2180–2192. https://doi.org/10.1038/ismej.2014.71.

Lu, M., Lu, Y., Ikejiri, T., Sun, D., Carroll, R., Blair, E.H., Algeo, T.J., Sun, Y., 2021. Periodic oceanic euxinia and terrestrial fluxes linked to astronomical forcing during the Late Devonian Frasnian-Famennian mass extinction. Earth Planet. Sci. Lett. 562, 116839 https://doi.org/10.1016/j.epsl.2021.116839.

MacLean, B.C., 2011. Tectonic and stratigraphic evolution of the Cambrian basin of northern Northwest Territories. Bull. Can. Petrol. Geol. 59, 172–194. https://doi.org/10.2113/gscpgbull.59.2.172.

MacLean, B.C., Fallas, K.M., Hadlari, T., 2014. The multi-phase Keele Arch, central Mackenzie Corridor, Northwest Territories. Bull. Can. Petrol. Geol. 62, 68–104. https://doi.org/10.2113/gscpgbull.62.2.68.

Madigan, M.T., 1995. Microbiology of nitrogen fixation by anoxygenic photosynthetic bacteria. In: Blankenship, R.E., Madigan, M.T., Bauer, C.E. (Eds.), Anoxygenic Photosynthetic Bacteria. Advances in Photosynthesis and Respiration. Springer, Dordrecht.

Mayer, B., Boyer, E.W., Goodale, C., Jaworski, N.A., Van Breemen, N., Howarth, R.W., Seitzinger, S., Billen, G., Lajtha, K., Nadelhoffer, K., Van Dam, D., Hetling, L.J., Nosal, M., Paustian, K., 2002. Sources of nitrate in rivers draining sixteen watersheds in the northeastern U.S.: isotopic constraints. In: Boyer, E.W., Howarth, R.W. (Eds.), The Nitrogen Cycle at Regional to Global Scales. Springer, Netherlands, Dordrecht, pp. 171–197. https://doi.org/10.1007/978-94-017-3405-9_5.

Mazzotti, S., Hyndman, R.D., 2002. Yakutat collision and strain transfer across the northern Canadian Cordillera. Geology 30, 495–498. https://doi.org/10.1130/0091-7613(2002)030<0495:YCASTA>2.0.CO;2.

McGhee, G.R., Clapham, M.E., Sheehan, P.M., Bottjer, D.J., Droser, M.L., 2013. A new ecological-severity ranking of major Phanerozoic biodiversity crises. Palaeogeogr. Palaeoclimatol. Palaeoecol. 370, 260–270. https://doi.org/10.1016/j.palaeo.2012.12.019.

Meyers, P.A., 1994. Preservation of elemental and isotopic source identification of sedimentary organic matter. Chem. Geol. 114, 289–302. https://doi.org/10.1016/0009-2541(94)90059-0.

Meyers, P.A., Eadie, B.J., 1993. Sources, degradation and recycling of organic matter associated with sinking particles in Lake Michigan. Org. Geochem. 20, 47–56. https://doi.org/10.1016/0146-6380(93)90080-U.

Minagawa, M., Wada, E., 1986. Nitrogen isotope ratios of red tide organisms in the East China Sea: a characterization of biological nitrogen fixation. Mar. Chem. 19, 245–259. https://doi.org/10.1016/0304-4203(86)90026-5.

Montoya, J.P., Carpenter, E.J., Capone, D.G., 2002. Nitrogen fixation and nitrogen isotope abundances in zooplankton of the oligotrophic North Atlantic. Limnol. Oceanogr. 47, 1617–1628. https://doi.org/10.4319/lo.2002.47.6.1617.

Morrow, D.W., 2018. Devonian of the Northern Canadian mainland Sedimentary Basin: a review. Bull. Can. Petrol. Geol. 66, 623–694.

Muir, I., Dixon, O.A., 1984. Facies analysis of a Middle Devonian sequence in the Mountain River-Gayna River. In: Brophy, J. (Ed.), Contributions to the Geology of the Northwest Territories. Department of Indian Affairs and Northern Development, Canada., pp. 55–62

Muir, I., Wong, P., Wendte, J., 1985. Devonian Hare Indian-Ramparts (Kee Scarp) evolution, Mackenzie Mountains and subsurface Norman Wells, NWT: basin-fill and platform reef development. In: Longman, M.W., Shanley, K.W., Lindsay, R.F., Eby, D. E. (Eds.), Rocky Mountain Carbonate Reservoirs: A Core Workshop. SEPM (Society for Sedimentary Geology), pp. 311–341. https://doi.org/10.2110/cor.85.07.

Murphy, A.E., Sageman, B.B., Hollander, D.J., 2000. Eutrophication by decoupling of the marine biogeochemical cycles of C, N, and P: a mechanism for the Late Devonian mass extinction. Geology 28, 427–430. https://doi.org/10.1130/0091-7613(2000)28<427:EBDOTM>2.0.CO;2.

Norris, A.W., 1985. Stratigraphy of Devonian outcrop belts in northern Yukon Territory and northwestern District of Mackenzie (Operation Porcupine area) (Memoir No. 410). Geological Survey of Canada. https://doi.org/10.4095/120309.

O'Leary, M.H., 1981. Carbon isotope fractionation in plants. Phytochemistry 20, 553–567. https://doi.org/10.1016/0031-9422(81)85134-5.

Ormiston, A.R., Oglesby, R.J., 1995. Effect of Late Devonian Paleoclimate on Source Rock Quality and Location. In: Huc, A.-Y. (Ed.), Paleogeography, Paleoclimate, and Source Rocks. American Association of Petroleum Geologists. https://doi.org/10.1306/St40595C5.

Pennock, J.R., Velinsky, D.J., Ludlam, J.M., Sharp, J.H., Fogel, M.L., 1996. Isotopic fractionation of ammonium and nitrate during uptake by Skeletonema costatum: implications for δ15N dynamics under bloom conditions. Limnol. Oceanogr. 41, 451–459. https://doi.org/10.4319/lo.1996.41.3.0451.

Pisarzowska, A., Racki, G., 2012. Isotopic chemostratigraphy across the Early-Middle Frasnian transition (Late Devonian) on the south polish carbonate shelf: a reference for the global punctata event. Chem. Geol. 334, 199–220. https://doi.org/10.1016/j.chemgeo.2012.10.034.

Powell, J.W., Issler, D.R., Schneider, D.A., Fallas, K.M., Stockli, D.F., 2020. Thermal history of the Mackenzie Plain, Northwest Territories, Canada: insights from low-temperature thermochronology of the Devonian Imperial Formation. GSA Bull. 132, 767–783. https://doi.org/10.1130/B35089.1.

Prahl, F.G., De Lange, G.J., Scholten, S., Cowie, G.L., 1997. A case of post-depositional aerobic degradation of terrestrial organic matter in turbidite deposits from the Madeira Abyssal Plain. Org. Geochem. Organic Geochemistry of Paleoclimatic Markers: Production, Preservation and Modeling 27, 141–152. https://doi.org/10.1016/S0146-6380(97)00078-8.

Pugh, D.C., 1983. Pre-Mesozoic geology in the subsurface of Peel River map area, Yukon Territory and district of Mackenzie (Memoir No. 401). Geological Survey of Canada. https://doi.org/10.4095/119498.

Pyle, L.J., Gal, L.P., 2016. Reference section for the Horn River group and definition of the Bell Creek Member, Hare Indian Formation in Central Northwest territories. Bull. Can. Petrol. Geol. 64, 67–98. https://doi.org/10.2113/gscpgbull.64.1.67.

Pyle, L.J., Gal, L.P., Fiess, K.M., 2014. Devonian Horn River Group: A Reference Section, Lithogeochemical Characterization, Correlation of Measured Sections and Wells, and Petroleum-Potential Data, Mackenzie Plain area (NTS 95M, 95N, 96C, 96D, 96E, 106H, and 106I), NWT (NWT Open File No. 2014– 06).

Racki, G., Rakociński, M., Marynowski, L., Wignall, P.B., 2018. Mercury enrichments and the Frasnian-Famennian biotic crisis: a volcanic trigger proved? Geology 46, 543–546. https://doi.org/10.1130/G40233.1.

Rivera, K.T., Puckette, J., Quan, T.M., 2015. Evaluation of redox versus thermal maturity controls on δ 15 N in organic rich shales: a case study of the Woodford Shale, Anadarko Basin, Oklahoma,USA. Org. Geochem. 83–84, 127–139. https://doi.org/10.1016/j.orggeochem.2015.03.005.

Robinson, R.S., Kienast, M., Albuquerque, A.L., Altabet, M., Contreras, S., Holz, R.D.P., Dubois, N., Francois, R., Galbraith, E., Hsu, T.-C., Ivanochko, T., Jaccard, S., Kao, S.-J., Kiefer, T., Kienast, S., Lehmann, M., Martinez, P., McCarthy, M., Möbius, J., Pedersen, T., Quan, T.M., Ryabenko, E., Schmittner, A., Schneider, R., Schneider-Mor, A., Shigemitsu, M., Sinclair, D., Somes, C., Studer, A., Thunell, R., Yang, J.-Y., 2012. A review of nitrogen isotopic alteration in marine sediments. Paleoceanography 27. https://doi.org/10.1029/2012PA002321.

Sackett, W.M., 1989. The Marine environment, A. In: Fritz, P., Fontes, J.C. (Eds.), Handbook of Environmental Isotope Geochemistry. Elsevier Scientific PubCo, Amsterdam, pp. 139–169.

Schelske, C.L., Hodell, D.A., 1995. Using carbon isotopes of bulk sedimentary organic matter to reconstruct the history of nutrient loading and eutrophication in Lake Erie. Limnol. Oceanogr. 40, 918–929. https://doi.org/10.4319/lo.1995.40.5.0918.

Scotese, C.R., 2014. Atlas of Devonian Paleogeographic Maps, PALEOMAP Atlas for ArcGIS, volume 4, The Late Paleozoic, Maps 65-72, Molleweide Projection.

Scotese, C.R., McKerrow, W.S., 1990. Revised World maps and introduction. Geol. Soc. Lond. Mem. 12, 1–21. https://doi.org/10.1144/GSL.MEM.1990.012.01.01.

Snowdon, L.R., Brooks, P.W., Williams, G.K., Goodarzi, F., 1987. Correlation of the Canol Formation source rock with oil from Norman Wells. Org. Geochem. 11, 529–548. https://doi.org/10.1016/0146-6380(87)90008-8.

Tang, Y., Huang, Y., Ellis, G.S., Wang, Y., Kralert, P.G., Gillaizeau, B., Ma, Q., Hwang, R., 2005. A kinetic model for thermally induced hydrogen and carbon isotope fractionation of individual n-alkanes in crude oil. Geochim. Cosmochim. Acta 69, 4505–4520. https://doi.org/10.1016/j.gca.2004.12.026.

Tassonyi, E.J., 1969. Subsurface geology, lower Mackenzie River and Anderson River area, District of Mackenzie (Paper No. 68–25). Geological Survey of Canada.

Terlaky, V., Fiess, K.M., Rocheleau, J.M., 2020. Outcrop description, lithogeochemical, and source-rock characterisation of the Devonian Horn River Group at the Arctic Red River East and Flyaway Creek outcrops – NTS 106F and 106G, Northwest Territories (No. NWT Open Report 2019-004).

Thunell, R.C., Sigman, D.M., Muller-Karger, F., Astor, Y., Varela, R., 2004. Nitrogen isotope dynamics of the Cariaco Basin,Venezuela. Glob. Biogeochem. Cycles 18. https://doi.org/10.1029/2003GB002185.

Tissot, B.P., Welte, D.H., 1984. Petroleum Formation and Occurrence, 2nd ed. Springer-Verlag, Berlin, New York.

Tocqué, E., Behar, F., Budzinski, H., Lorant, F., 2005. Carbon isotopic balance of kerogen pyrolysis effluents in a closed system. Org. Geochem. 36, 893–905. https://doi.org/10.1016/j.orggeochem.2005.01.007.

Uveges, B.T., Junium, C.K., Scholz, C.A., Fulton, J.M., 2020. Chemocline collapse in Lake Kivu as an analogue for nitrogen cycling during Oceanic Anoxic events. Earth Planet. Sci. Lett. 548, 116459 https://doi.org/10.1016/j.epsl.2020.116459.

Voss, M., Deutsch, B., Elmgren, R., Humborg, C., Kuuppo, P., Pastuszak, M., Rolff, C., Schulte, U., 2006. Source identification of nitrate by means of isotopic tracers in the Baltic Sea catchments. Biogeosciences 3, 663–676. https://doi.org/10.5194/bg-3-663-2006.

Wada, E., Kabaya, Y., Tsuru, K., Ishiwatari, R., 1990. 13C and 15N abundance of sedimentary organic matter in estuarine areas of Tokyo Bay,Japan. Mass Spectrosc 38, 307–318.

Walliser, O.H., 1996. Global events in the Devonian and Carboniferous. In: Walliser, O.H. (Ed.), Global Events and Event Stratigraphy in the Phanerozoic. Springer, Berlin Heidelberg, pp. 225–250.

Williams, L.B., Ferrell, R.E., Hutcheon, I., Bakel, A.J., Walsh, M.M., Krouse, H.R., 1995. Nitrogen isotope geochemistry of organic matter and minerals during diagenesis and hydrocarbon migration. Geochim. Cosmochim. Acta 59, 765–779. https://doi.org/10.1016/0016-7037(95)00005-K.

Wilson, G.P., Lamb, A.L., Leng, M.J., Gonzalez, S., Huddart, D., 2005. Variability of organic δ13C and C/N in the Mersey Estuary, U.K. And its implications for sea-level reconstruction studies. Estuar. Coast. Shelf Sci. 64, 685–698. https://doi.org/10.1016/j.ecss.2005.04.003.

Yose, L.A., Brown, S., Davis, T.L., Eiben, T., Kompanik, G.S., Maxwell, S.R., 2001. 3-D geologic model of a fractured carbonate reservoir, Norman Wells Field, NWT, Canada. Bull. Can. Pet. Geol. 49, 86–116. https://doi.org/10.2113/49.1.86.

Zambito, J.J., Brett, C.E., Baird, G.C., 2012. The Late Middle Devonian (Givetian) Global Taghanic Biocrisis in its type area (Northern Appalachian Basin): geologically rapid faunal transitions driven by global and local environmental changes. In: Talent, J.A. (Ed.), Earth and Life: Global Biodiversity, Extinction Intervals and Biogeographic Perturbations through Time. Springer, Netherlands.

Zhang, X., Joachimski, M.M., Over, D.J., Ma, K., Huang, C., Gong, Y., 2019. Late Devonian carbon isotope chemostratigraphy: a new record from the offshore facies of South China. Glob. Planet. Change 182, 103024. https://doi.org/10.1016/j.gloplacha.2019.103024.